

# A Phase-controlled Stacked-transmitter Wireless Power Transfer System for Magnetic Field Beamforming

1<sup>st</sup> Ning Kang

*University of Michigan-Shanghai  
Jiao Tong University Joint Institute,  
Shanghai Jiao Tong University,  
Shanghai, China  
corningkdc@sjtu.edu.cn*

2<sup>nd</sup> Ming Liu

*Department of Electrical Engineering,  
Princeton University,  
Princeton, US  
ml45@princeton.edu*

3<sup>rd</sup> Chengbin Ma

*University of Michigan-Shanghai  
Jiao Tong University Joint Institute,  
Shanghai Jiao Tong University,  
Shanghai, China  
chbma@sjtu.edu.cn*

**Abstract**—Wireless power transfer (WPT) systems operating in MHz have the advantages of small size and a high tolerance for coil misalignment. Existing MHz WPT systems are urgently needed to increase transmission distance and coupling coils efficiency. Although there are some methods for improving the transmission distance and coils efficiency, such as introduced repeaters coils and using the special coils structures. However, the lack of magnetic field strength often limits the transmission distance of the WPT system, and the excessive coupling coefficient can cause inefficiencies in the coupling coils. This paper proposes a compact 2-D stacked-transmitter structure to shape the 3-D magnetic field so as to maximize the transmission distance and coils efficiency. Only the phase angle difference of the drive signals is controlled, and the parameters of compensation capacitors for compensating the cross coupling are designed. The experimental results are in good agreement with the theoretical analysis and simulation. Therefore, a stacked transmitter WPT system with phase angle control has advantages in terms of transmission distance and coupling coil efficiency compared to a single transmitter WPT system.

**Index Terms**—wireless power transfer, MHz, phase angle control, stacked-transmitter

## I. INTRODUCTION

Wireless power transfer (WPT) is a convenient, simple, and secure technology for many applications from consumer electronics to electric vehicles. In general, there is a fundamental tradeoff between transmission distance and coupling coils efficiency in WPT system: when the transmission distance is short, the energy transfer efficiency is high because the coupling is strong; while when increasing the transmission distance, the coupling coefficient decreases rapidly results in lower efficiency [1]. To better deal with the conflict between efficiency and distance WPT system, the researchers have done a lot of works. Since the transmission distance of magnetic induction coupling systems is usually short, previous studies have introduced magnetic resonance coupling systems to increase the transmission distance [2]. In recent years, several studies introduced repeaters between the transmitter and receiver coils [3]. New power electronics, such as power amplifiers, rectifier diodes, and DC-DC converters, have been

developed to increase energy transfer efficiency [4]. Besides, the coupling coefficient has been increased by using new material [5]. However, these methods have a limited effect on improving system performance and often introduce new problems, such as application scenario limitations and cost increases. For these reasons, magnetic field shaping technology has been attracting growing interest [6]–[8].

Magnetic field shaping technology allows control of the magnetic field strength and direction at a particular location and reduces excessive coupling coefficient; thereby increasing transmission distance and coupling coils efficiency simultaneously. Noted that both weak and excessive coupling are disadvantageous for WPT systems. When the coupling coefficient is small, the transmission distance of the WPT system will be limited. Conversely, an excessive coil coupling coefficient is also detrimental to the efficient and stable operation of the WPT system. The reason is that an excessive coupling coefficient will cause the power amplifier (PA) to see a large impedance, which is not conducive to the stable operation of the PA and the output of sufficient power. Moreover, the quality factor of the coil should be large enough for the coupling coils to operate stably in the case of strong coupling. Generally, the magnetic field shaping technology can be divided into two categories: passive methods and active methods. Passive methods introduce a magnetic core to provide a low reluctance path for the magnetic flux, but such an approach can significantly increase the size and weight of the transmitter and receiver [9]. The active method achieves magnetic field shaping by changing the distribution of current in the transmitters [7]. In order to improve the performance of WPT systems by shaping the magnetic field, some state-of-art techniques have been proposed [10], [11]. However, for avoiding cross coupling between the transmitting coils, the transmitting coils in these systems are designed to be bulky 3-D structures, which obviously limits the application scenarios of these systems. In addition, the coupling coils in these systems resonate at lower frequencies, which makes the power amplifier and rectifier larger in size.

The main idea of this paper is to effectively implement the 3-D magnetic field shaping technology in the MHz WPT system by using the compact 2-D stacked coils structure, thereby increasing the distance and efficiency of wireless energy transmission. This paper is organized as follows. Section II gives a circuit structure of the stacked-transmitter WPT system and analytically derives its expression of coils efficiency. Based on Biot-Savart law, section III develops the magnetic field generated by the single coil and the two stacked coils. Then section IV validates the analytical results by experiments using the example 6.78-MHz WPT system. The effects of cross coupling of the transmitting coils were carefully considered in simulations and experiments. Finally, section V draws the conclusions.

## II. STACKED-TRANSMITTER WPT SYSTEM

Fig. 1 shows the schematic of the proposed MHz WPT system with two transmitters and one receiver. The transmitter side comprises two current-mode class E power amplifiers operating at 6.78 MHz and two transmitting coils. The receiver side comprises a receiving coil and a class E full-wave rectifier. The phase difference between the drive signals of the two MOSFETs is adjustable. By controlling the phase difference between the two drive signals, the two transmitting coils will obtain different-phase currents. The two transmitting coils are stacked and fixed in position. In order to compensate the cross coupling at transmitting coils, the capacitors of two transmitters must be carefully adjusted so as to two power amplifiers both see pure resistive loads.

The input impedance of the class E full-wave rectifier,  $Z_{rec}$ , which can be represented as

$$Z_{rec} = R_{rec} + jX_{rec} \quad (1)$$

where  $R_{rec}$  is the resistance and  $X_{rec}$  is the reactance. In order to compensate for the reactance part of the rectifier, the optimal compensation capacitance of the receiving coil needs to satisfy the following relationship

$$j\omega L_{rx} + \frac{1}{j\omega C_{rx}} + jX_{rec} = 0 \quad (2)$$

where  $L_{rx}$  is the inductances of the receiving coil, and  $\omega$  is the resonance frequency of the WPT system, i.e., 6.78 MHz here [12]. Then the compensation capacitor of the receiving coil can be derived as

$$C_{rx} = \frac{1}{\omega(\omega L_{rx} + X_{rec})} \quad (3)$$

The impedance change caused by the change in the coupling coefficient ( $k$ ) detunes the resonance of the coupling coils and reduces the performance of the RF power amplifier. Here, we introduce an impedance compression method for the stacked-transmitter architecture to maintain high coupling coefficient variation performance. The specific structure is shown in the Pi-shaped network in Fig. 1.

In order to analyze the stacked-transmitter system (STS), we first need to know the input impedance and coil efficiency

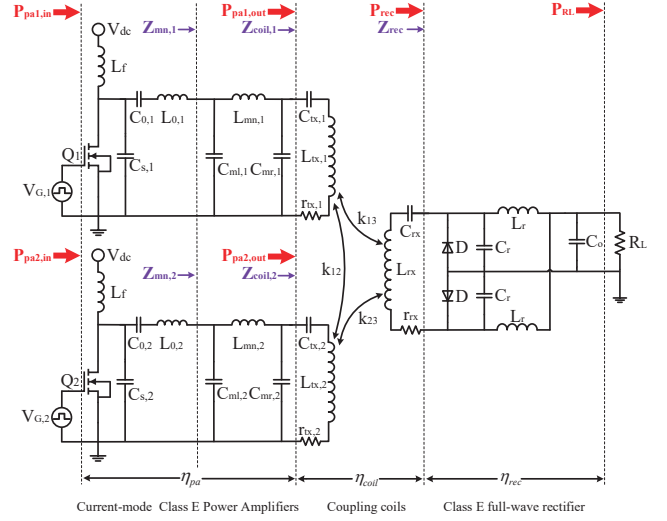


Fig. 1. Configuration of a stacked-transmitter wireless power transfer system.

of the coupling coils in the one transmitter system (OTS). For coupling coils, the power loss occurs on the parasitic resistances, i.e.,  $r_{tx}$  and  $r_{rx}$ . According to the derivation of [13], the input impedance of the coupling coils is

$$Z_{in} = r_{tx} + \frac{\omega^2 k^2 L_{rx} L_{tx}}{r_{rx} + R_{rec}} \quad (4)$$

For a pair of coupling coils, the transmission efficiency can be expressed as

$$\eta_{coil} = \eta_{tx} \eta_{cx} = \frac{\Re(Z_{in}) - r_{tx}}{\Re(Z_{in})} \frac{R_{rec}}{R_{rec} + R_{rec}} \quad (5)$$

where  $\Re(Z_{in})$  indicates the real part of the input impedance of the coupling coils.  $Z_{in}$  is purely resistive in the case of satisfying the optimum compensation capacitance. For simplicity, the transmitting and receiving coils are identical in our system. In this case, the following conditions are met:  $r_{tx} = r_{rx} = r$  and  $L_{tx} = L_{rx} = L$ . Thus the efficiency of a pair of coils (one transmitting coil and one receiving coil)  $\eta_{coil}$  can be rewritten as

$$\eta_{coil} = \frac{R_{rec}}{\left(1 + \frac{r(r+R_{rec})}{\omega^2 k^2 L^2}\right) (R_{rec} + r)} \quad (6)$$

Similarly, the impedance expression seen by each coil in the STS is shown as

$$Z_{ins} = r_{tx} + \frac{\omega^2 k^2 L_{rx} L_{tx}}{r_{rx} + R_{rec}} + \frac{\omega^2 k^2 L_{tx}^2}{r_{tx} + R_{pa}} \quad (7)$$

where  $R_{pa}$  represents the input impedance seen from the transmitting coil end of another PA. As in the previous conditions, all transmitting coils and receiving coil are identical. Then, the efficiency of the coils in the STS can be expressed as

$$\eta_{coils} = \frac{R_{rec}}{\left(1 + \frac{r(r+R_{rec})(r+R_{pa})}{(\omega^2 k^2 L^2)(2r+R_{pa}+R_{rec})}\right) (R_{rec} + r)} \quad (8)$$

Observe the different part of (6) and (8)

$$\frac{r + R_{pa}}{2r + R_{pa} + R_{rex}} < 1 \quad (9)$$

The above formula implies that the coil efficiency of the STS is greater than the coil efficiency of the OTS, which can be expressed as

$$\eta_{coils} > \eta_{coil} \quad (10)$$

In fact, the above conclusion can also be derived from a simple analysis. For one transmitting coil in STS, the coupling of the other transmitting coil increases the reflected impedance seen by the transmitting coil. According to (5) and (7), the energy transfer efficiency of the coupling coils will increase.

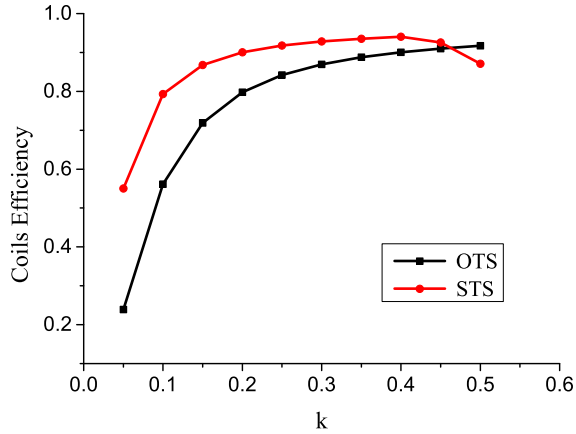


Fig. 2. Simulation results of coils efficiency in STS and OTS with the coupling coefficient changing from 0.05 to 0.5.

To quantify the advantages of STS in coil efficiency, we simulated STS and OTS with the Advanced Design System (ADS). In the simulation, the transmitting coils and the receiving coil are identical, where  $L = 1.244\mu\text{H}$  and  $r = 0.4\Omega$ . When the coupling coefficient ( $k$ ) is increased from 0.05 to 0.4, the coil efficiency of the STS has a significant advantage over the OTS. In particular, when  $k$  is small (when the transmission distance is long), the coil efficiency advantage of the STS is greater. This means that STS is more suitable for long-distance transmission than OTS. Note that when  $k > 0.45$ , the coil efficiency of the STS will decrease. As mentioned in the previous section, the impedance seen by the transmitting coil is very large in the case of large  $k$ , and the Q value of the coil is insufficient to support the normal operation of the coupling coils. However, in the actual system, when  $k$  is large, the corresponding transmission distance is quite short. Such transmission distances have little meaning for the MHz WPT system. In our experiments, the rectangular coil has a side length of 10cm and an inductance of 1.244  $\mu\text{H}$ . Only when the spacing of two opposite coils is less than 5mm, the coupling coefficient between the coils will be greater than 0.45.

### III. PHASE ANGLE CONTROL FOR MAGNETIC FIELD BEAMFORMING

According to the Biot-Savart law, the magnetic induction in space is defined as

$$B = \frac{\mu_0}{4\pi} \oint_C \frac{Idl \times r}{|r|^3} \quad (11)$$

where  $dl$  is a vector along the path  $C$  whose magnitude is the length of the differential element of the coil in the direction of current.  $r$  is the full displacement vector from the wire element ( $dl$ ) to the point at which the field is being computed, and  $\mu_0$  is the magnetic constant. Then, the magnetic field generated by a rectangular coil flowing through a sinusoidal current at a certain point can be expressed as

$$B_0 = \oint_C \frac{\mu_0 n I_0 \cos(\omega t)}{4\pi r^2} dl \times r \quad (12)$$

where  $n$  represents the number of turns of the coil and  $I_0$  is the magnitude of current in the coil. Decompose the loop integral into four straight line integrals, and the magnetic field component perpendicular to the plane of the coil can be expressed as

$$B_{z_1} = \frac{\mu_0 n I_0 \cos(\omega t)}{4\pi} (a - b + c - d) \quad (13)$$

where the parameters  $a$ ,  $b$ ,  $c$ , and  $d$  are four integral expressions as follow

$$a = \int_{2l}^0 \frac{y}{((x - x_1)^2 + y^2 + z^2)^{3/2}} dx_1 \quad (14)$$

$$b = \int_0^{2l} \frac{x}{(x^2 + (y - y_1)^2 + z^2)^{3/2}} dy_1 \quad (15)$$

$$c = \int_0^{2l} \frac{y - 2l}{((x - x_1)^2 + (y - 2l)^2 + z^2)^{3/2}} dx_1 \quad (16)$$

$$d = \int_{2l}^0 \frac{x - 2l}{((x - 2l)^2 + (y - y_1)^2 + z^2)^{3/2}} dy_1 \quad (17)$$

where  $2l$  represents the side length of the square coil. Similarly, the magnetic field strength produced by the other coil is expressed as

$$B_{z_2} = \frac{\mu_0 n I_0 \cos(\omega t + \theta)}{4\pi} (a - b + c - d) \quad (18)$$

On the other hand, the sum of the magnetic fields generated by the two coils in the vertical direction can be expressed as

$$B_z = B_{z_1} + B_{z_2} \quad (19)$$

According to (13), (18) and (19), the magnetic field generated by two stacked rectangular transmitting coils is

$$B_z = \frac{\mu_0 n I_0 (\cos(\omega t) + \cos(\omega t + \theta))}{4\pi} (e + f - g - h) \quad (20)$$

where  $n$  represents the same number of turns for the two coils,  $I_0$  is the same current amplitude in the two coils, and  $\theta$  is the phase difference of the currents in the two coils. In addition,

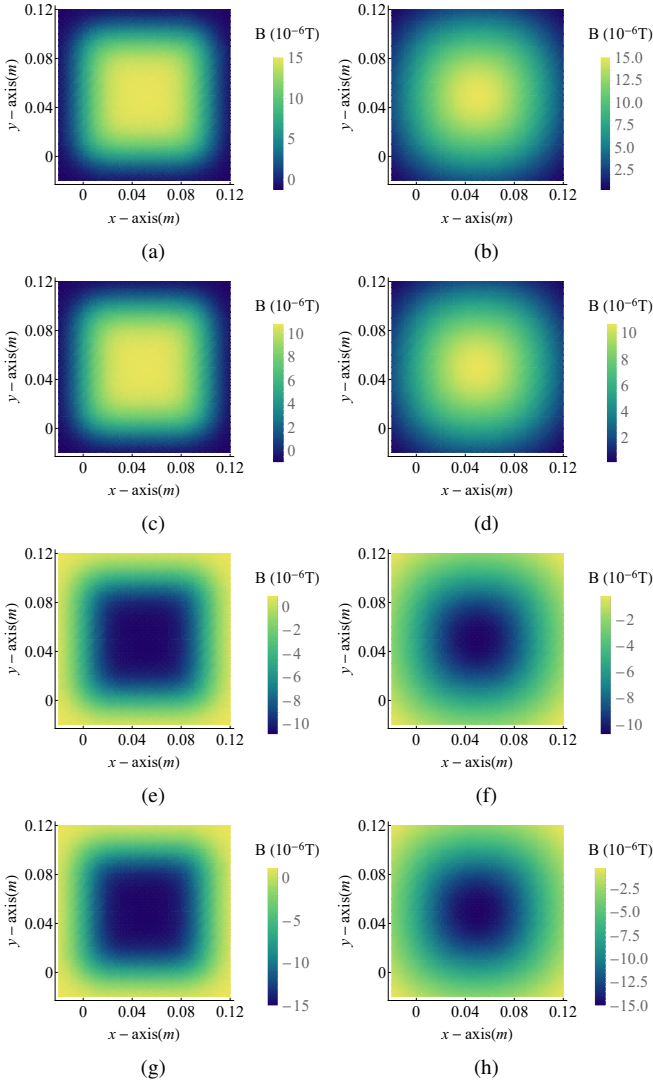


Fig. 3. Simulation results of B-field in different height levels at different time. (a) B-field of the single transmitting coil, where  $d=3.00\text{cm}$  and  $t=0$ . (b) B-field of the two stacked transmitting coils, where  $d=5.76\text{cm}$  and  $t=0$ . (c) B-field of the single transmitting coil, where  $d=3.00\text{cm}$  and  $t=\frac{\pi}{4}$ . (d) B-field of the two stacked transmitting coils, where  $d=5.76\text{cm}$  and  $t=\frac{\pi}{4}$ . (e) B-field of the single transmitting coil, where  $d=3.00\text{cm}$  and  $t=\frac{3\pi}{4}$ . (f) B-field of the two stacked transmitting coils, where  $d=5.76\text{cm}$  and  $t=\frac{3\pi}{4}$ . (g) B-field of the single transmitting coil, where  $d=3.00\text{cm}$  and  $t=\pi$ . (h) B-field of the two stacked transmitting coils, where  $d=5.76\text{cm}$  and  $t=\pi$ .

the four parameters  $e$ ,  $f$ ,  $g$ , and  $h$  are determined by the spatial position coordinates, which can be represented as follows

$$e = \frac{y \left( -\frac{x}{\sqrt{x^2+y^2+z^2}} + \frac{-2l+x}{\sqrt{(-2l+x)^2+y^2+z^2}} \right)}{y^2 + z^2} \quad (21)$$

$$f = \frac{x \left( -\frac{y}{\sqrt{x^2+y^2+z^2}} + \frac{-2l+y}{\sqrt{x^2+(-2l+y)^2+z^2}} \right)}{x^2 + z^2} \quad (22)$$

$$g = \frac{(y-2l) \left( \frac{-2l+x}{\sqrt{(x-2l)^2+(y-2l)^2+z^2}} - \frac{x}{\sqrt{x^2+(y-2l)^2+z^2}} \right)}{(-2l+y)^2 + z^2} \quad (23)$$

$$h = \frac{(x-2l) \left( \frac{y-2l}{\sqrt{(x-2l)^2+(y-2l)^2+z^2}} - \frac{y}{\sqrt{(x-2l)^2+y^2+z^2}} \right)}{(x-2l)^2 + z^2} \quad (24)$$

In the simulation, the two transmitting coils are stacked on an  $xy$  plane with a  $z$  coordinate of zero.

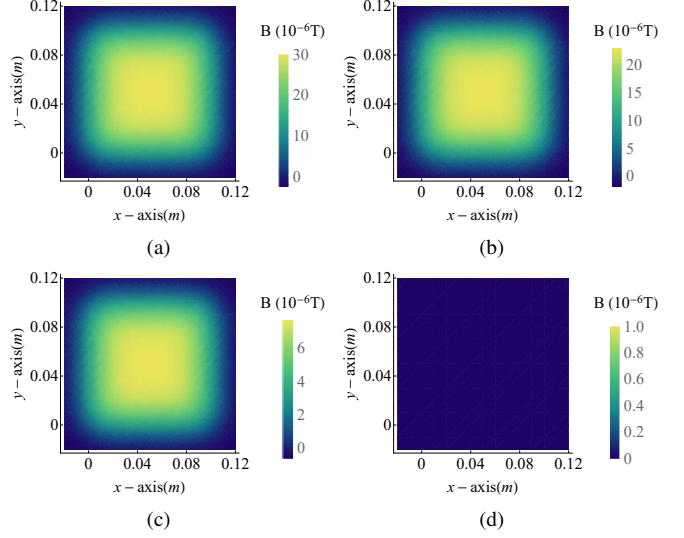


Fig. 4. Simulation results of B-field generated by two stacked transmitting coils with different phase differences ( $d=3.00\text{cm}$ ,  $t=0$ ). (a) B-field of  $\theta=0$ . (b) B-field of  $\theta=60^\circ$ . (c) B-field of  $\theta=120^\circ$ . (d) B-field of  $\theta=180^\circ$ .

According to the above equations, we can systematically compare the difference between the magnetic fields generated by the stacked-transmitting coils as well as the single transmitting coil. Then, the magnetic field generated by the stacked transmitting coils at different phase differences can be studied. Fig. 3 shows the simulation results of magnetic induction distribution (B-field) in different height levels at different time, where  $d$  means the height of the horizontal plane from the transmitting coils. For the two figures in each row, both figures have the same maximum magnetic field strength. However, multiple transmitting coils can produce the same intensity magnetic fields at a farther distance, which implies that the multiple transmitting coils have farther energy transmission distances. Fig. 4 shows the simulation results of B-field generated by two stacked transmitting coils with different phase differences when  $d=3.00\text{cm}$  and  $t=0$ . As the phase difference increases, the strength of the magnetic field gradually decreases until it approaches zero. The strength of the magnetic field at the fixed height can be changed by changing the phase difference of the current in the transmitting coils, thereby increasing the energy obtained by the receiving coil or avoiding the over-coupling at a short distance. In addition, changing the phase difference can also adjust the impedance seen by each power amplifier, allowing the power amplifier to operate in a more ideal state.

#### IV. EXPERIMENTAL RESULTS

Fig. 5 shows a prototype stacked-transmitter WPT system comprising two current-mode class E power amplifier, two stacked transmitting coils, a receiving coil, and a class E full-wave rectifier. The circuit model of the two transmitters is the same and given in Fig. 1. In order to achieve better phase control performance, the parameters of the two PAs in the experimental system are chosen to be as same as possible. The two MHz frequency switches are MOSFETs(SUD15N15). The resonant frequency of the coils is 6.78 MHz. And the compensation capacitances of two transmitting coils are 303 pF and 313 pF, respectively. Based on the stacked-transmitter WPT architecture, the proposed magnetic field beamforming methods can be experimentally verified.

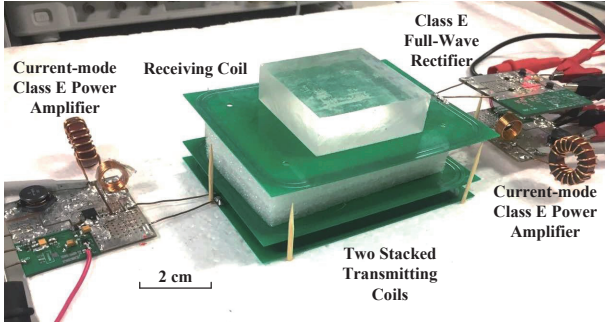


Fig. 5. A prototype stacked-transmitter WPT system with phase angle control.

The experimental waveforms (the drain voltages of the switches) of the three PAs in the STS and OTS under different  $d$  are shown in Fig. 6. The PA parameters of STS and OTS are optimized to the best. And the PA supply voltages of STS and OTS are the same. It can be seen that the three PAs operate in a high-efficiency soft switching state at different transmission distances, except that the second PA of the STS has a relatively large loss in the case of a short transmission distance. The reason for selecting only the waveforms under three transmission distances is to ensure the clarity of the image. Under other transmission distances, the PAs still work in the soft switching state. The receiving coil, the rectifier circuit and the DC load of the STS and OTS are identical. Thus, the system efficiency advantages of the STS relative to the OTS in Fig. 7(a) are mainly due to the stacked coils structure of the STS. As shown in Fig. 7(a), STS has significant system efficiency advantages over OTS at different transmission distances. Since the efficiency of the entire system is the product of the efficiencies of each part of the system, the advantage of the STS in coils efficiency is more obvious than its advantage in system efficiency. Note that the STS's system efficiency advantages are even more pronounced as the transmission distance increases. Fig. 7(b) gives the experimental and simulated results of the output DC power in STS and OTS. The estimated output DC power matches well with the measured power reported by the electronic load. Note that at each test distance, the output power of the STS is

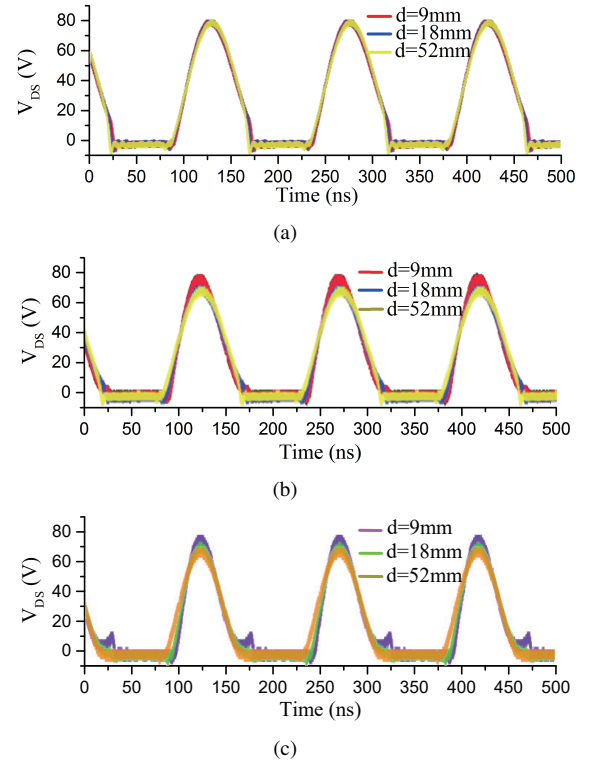


Fig. 6. The experimental waveforms (the drain voltages  $V_{DS}$  of the switches) of the three PAs in STS and OTS under different  $d$ . (a) The PA in the OTS. (b) The first PA in the STS. (c) The second PA in the STS.

four times the output power of the OTS. Furthermore, at the same output power level, the STS has approximately twice the energy transmission distance relative to the OTS. Therefore, both experimental results and simulation results demonstrate that STS has significant advantages over OTS in terms of power capacity or transmission distance.

TABLE I  
THE OPTIMIZED DRIVE PHASE DIFFERENCES OF PAs IN STS WITH DIFFERENT TRANSMISSION DISTANCES

Distance (mm)	9	18	26	35	44	52
Optimized $\theta$ (Degree)	-14	-13	-9	-8	-7	-7

Table I shows the optimized drive phase differences of PAs in STS at different transmission distances. Under such circumstances, the phase difference between the two driving signals is about  $-10^\circ$ . Note that in the magnetic field simulation, the magnetic field of the maximum intensity can be formed when the phase difference between the two transmitting coils is zero. The difference between simulation results and experimental results is caused by the different parameters of two PAs.

#### V. CONCLUSIONS

This paper presented a compactly 2-D stacked-transmitter structure to shape the 3-D magnetic field so as to maximize

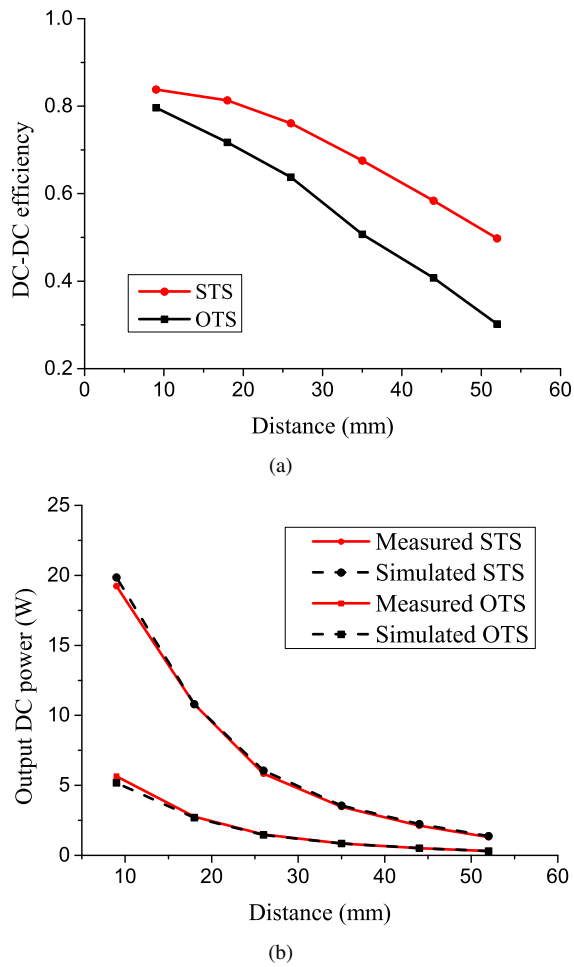


Fig. 7. Experimental results with the transmission distance changing from 9 mm to 52 mm. (a) The system efficiency of the STS and OTS. (b) The output performance of the STS and OTS.

the transmission distance and the efficiency of the coils. The circuit architecture is developed based on a WPT system with a constant current source PA. And the architecture can adjust the equivalent load seen by the two PAs by controlling the phase difference between the two drive signals. We developed the theory of magnetic field beamforming for stacked coils and proposed a method to increase the transmission distance and transmission efficiency. An STS and an OTS have been implemented to verify the effectiveness of the magnetic field beamforming method. In simulation and experimentation, STS has obvious advantages in terms of efficiency and transmission distance relative to OTS.

## VI. ACKNOWLEDGMENT

This work was supported by the Shanghai Natural Science Foundation under Grant 16ZR1416300. The authors would like to thank the Shanghai Natural Science Committee.

## REFERENCES

- [1] A. Karalis, J. D. Joannopoulos, and M. Soljačić, "Efficient wireless non-radiative mid-range energy transfer," *Annals of physics*, vol. 323, no. 1, pp. 34–48, 2008.
- [2] A. P. Sample, D. T. Meyer, and J. R. Smith, "Analysis, experimental results, and range adaptation of magnetically coupled resonators for wireless power transfer," *IEEE Transactions on industrial electronics*, vol. 58, no. 2, pp. 544–554, 2011.
- [3] T. Imura, "Equivalent circuit for repeater antenna for wireless power transfer via magnetic resonant coupling considering signed coupling," in *Industrial Electronics and Applications (ICIEA), 2011 6th IEEE Conference on*. IEEE, 2011, pp. 1501–1506.
- [4] W. Chen, R. Chinga, S. Yoshida, J. Lin, C. Chen, and W. Lo, "A 25.6 w 13.56 mhz wireless power transfer system with a 94% efficiency gan class-e power amplifier," in *2012 IEEE/MTT-S International Microwave Symposium Digest*. IEEE, 2012, pp. 1–3.
- [5] Y. Moriwaki, T. Imura, and Y. Hori, "Basic study on reduction of reflected power using dc/dc converters in wireless power transfer system via magnetic resonant coupling," in *IEEE 33rd International Telecommunications Energy Conference (INTELEC), 2011*, pp. 1–5.
- [6] L. C. Godara, "Application of antenna arrays to mobile communications. ii. beam-forming and direction-of-arrival considerations," *Proceedings of the IEEE*, vol. 85, no. 8, pp. 1195–1245, 1997.
- [7] W. Ahn, S. Jung, W. Lee, S. Kim, J. Park, J. Shin, H. Kim, and K. Koo, "Design of coupled resonators for wireless power transfer to mobile devices using magnetic field shaping," in *Electromagnetic Compatibility (EMC), 2012 IEEE International Symposium on*. IEEE, 2012, pp. 772–776.
- [8] H. Halbauer, S. Saur, J. Koppenborg, and C. Hoek, "3d beamforming: Performance improvement for cellular networks," *Bell Labs Technical Journal*, vol. 18, no. 2, pp. 37–56, 2013.
- [9] S. Santalunai, C. Thongsopa, and T. Thosdeekoraphat, "An increasing the power transmission efficiency of flat spiral coils by using ferrite materials for wireless power transfer applications," in *2014 11th International Conference on Electrical Engineering/Electronics, Computer, Telecommunications and Information Technology (ECTI-CON)*. IEEE, 2014, pp. 1–4.
- [10] Y. Lim and J. Park, "A novel phase-control-based energy beamforming techniques in nonradiative wireless power transfer," *IEEE Transactions on Power Electronics*, vol. 30, no. 11, pp. 6274–6287, 2015.
- [11] Q. Zhu, M. Su, Y. Sun, W. Tang, and A. P. Hu, "Field orientation based on current amplitude and phase angle control for wireless power transfer," *IEEE Transactions on Industrial Electronics*, vol. 65, no. 6, pp. 4758–4770, 2018.
- [12] M. Fu, T. Zhang, C. Ma, and X. Zhu, "Efficiency and optimal loads analysis for multiple-receiver wireless power transfer systems," *IEEE Transactions on Microwave Theory and Techniques*, vol. 63, no. 3, pp. 801–812, 2015.
- [13] M. Liu, M. Fu, and C. Ma, "Parameter design for a 6.78-mhz wireless power transfer system based on analytical derivation of class e current-driven rectifier," *IEEE Transactions on Power Electronics*, vol. 31, no. 6, pp. 4280–4291, 2016.